Cell Metabolism

Resource

Quantitative Fluxomics of Circulating Metabolites

Graphical Abstract

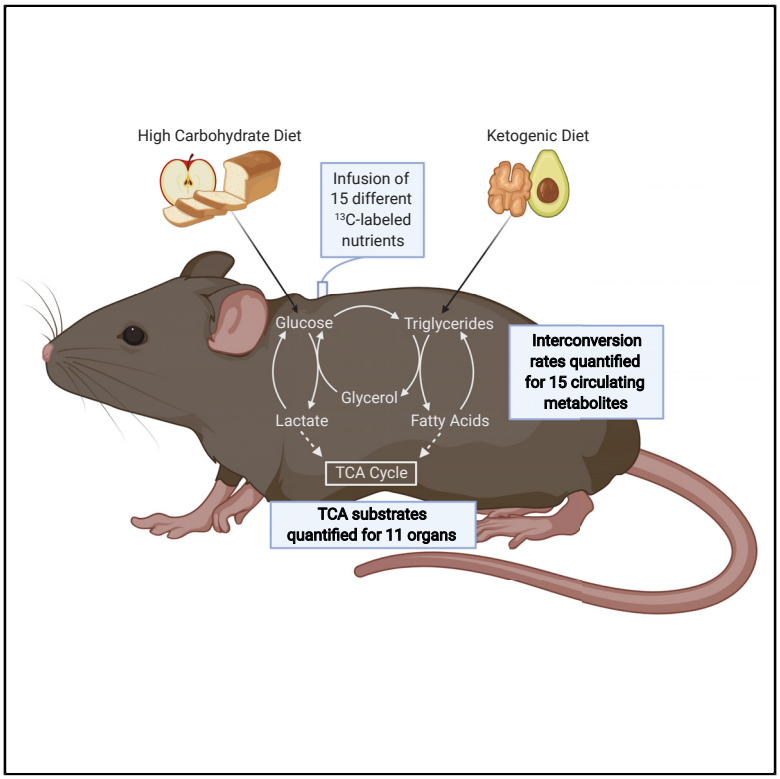

Highlights

- Comprehensive isotope tracer studies reveal TCA substrate usage for 11 major organs
- These data also reveal interconversion rates between circulating nutrients
- Circulatory fluxes are similar across high-carbohydrate and ketogenic diet
- Futile cycling helps render internal metabolic activity robust to food choice

Authors

Sheng Hui, Alexis J. Cowan, Xianfeng Zeng, ..., Jennifer Rojas, Joseph Baur, Joshua D. Rabinowitz

Correspondence

shui@hsph.harvard.edu (S.H.), joshr@princeton.edu (J.D.R.)

In Brief

By infusing 15 different ^{13}C-isotope tracers, Hui et al. quantify metabolic fluxes in mice on either high-carbohydrate or ketogenic diet. Results include interconversion fluxes between circulating metabolites and their contributions to the TCA cycle in 11 major organs. Rapid interconversion among circulating carbon carriers renders internal metabolic activity robust to diet.

Hui et al., 2020, Cell Metabolism *32*, 676–688
October 6, 2020
https://doi.org/10.1016/j.cmet.2020.07.013

CellPress

CellPress

Cell Metabolism

Resource

Quantitative Fluxomics of Circulating Metabolites

Sheng Hui,[1,2,4,5,*] Alexis J. Cowan,[1,4] Xianfeng Zeng,[1] Lifeng Yang,[1] Tara TeSlaa,[1] Xiaoxuan Li,[1] Caroline Bartman,[1] Zhaoyue Zhang,[1] Cholsoon Jang,[1] Lin Wang,[1] Wenyun Lu,[1] Jennifer Rojas,[3] Joseph Baur,[3] and Joshua D. Rabinowitz[1,6,*]

[1]Lewis Sigler Institute for Integrative Genomics and Department of Chemistry, Princeton University, Washington Road, Princeton, NJ 08544, USA

[2]Department of Molecular Metabolism, Harvard T. H. Chan School of Public Health, 655 Huntington Avenue, Boston, MA 02115, USA

[3]Department of Physiology and Institute for Diabetes, Obesity, and Metabolism, Perelman School of Medicine, University of Pennsylvania, 3400 Civic Boulevard, Philadelphia, PA 19104, USA

[4]These authors contributed equally

[5]Twitter: @realTonyHui

[6]Lead Contact

*Correspondence: shui@hsph.harvard.edu (S.H.), joshr@princeton.edu (J.D.R.)

https://doi.org/10.1016/j.cmet.2020.07.013

SUMMARY

Mammalian organs are nourished by nutrients carried by the blood circulation. These nutrients originate from diet and internal stores, and can undergo various interconversions before their eventual use as tissue fuel. Here we develop isotope tracing, mass spectrometry, and mathematical analysis methods to determine the direct sources of circulating nutrients, their interconversion rates, and eventual tissue-specific contributions to TCA cycle metabolism. Experiments with fifteen nutrient tracers enabled extensive accounting for both circulatory metabolic cycles and tissue TCA inputs, across fed and fasted mice on either high-carbohydrate or ketogenic diet. We find that a majority of circulating carbon flux is carried by two major cycles: glucose-lactate and triglyceride-glycerol-fatty acid. Futile cycling through these pathways is prominent when dietary content of the associated nutrients is low, rendering internal metabolic activity robust to food choice. The presented *in vivo* flux quantification methods are broadly applicable to different physiological and disease states.

INTRODUCTION

As animals, we get our nutrients from the food we eat. Tissues in our body, however, do not take their nutrients directly from food. Instead, they acquire nutrients from the blood circulation. Tissues must continuously burn circulating nutrients, but animals do not consume food all the time. To resolve this mismatch, in the simplest scenario, animals store dietary nutrients in fed state and utilize the stored nutrients in fasted state (Figure 1A). Decades of research support this basic model, for example showing that after feeding, insulin drives glucose storage as glycogen, while during fasting glucagon promotes release of glycogen to maintain blood glucose levels (Frayn, 2009; Newsholme and Leech, 2011).

At the same time, beyond simply being stored, released, and burned, circulatory metabolites are interconnected. For example, in addition to its direct production by the breakdown of hepatic glycogen, circulating glucose is also maintained during fasting by synthesis from lactate released by muscle. This glucose can then be used by muscle as fuel, creating a loop known as the Cori cycle (Frayn, 2009; Newsholme and Leech, 2011). Similarly, the Cahill cycle describes the interconversion between glucose and alanine (Felig, 1973). Another example is the glucose-glycerol interconnection in the triglyceride-fatty acid cycle, wherein the glycerol released by the breakdown of triglycerides can be used for glucose production and the glycerol backbone in the re-synthesized triglycerides can come from glucose (Reshef et al., 2003).

While there has been a great deal of progress in understanding these metabolic pathways and their regulation, it remains unclear whether metabolism largely follows the simple logic of nutrient storage, release, and burning, or whether interconversion of circulating metabolites is a major quantitative feature. Moreover, as animals make divergent food choices (e.g., a diet high in carbohydrate versus a diet high in fat), the impact on internal metabolic activities remains substantially to be elucidated.

Here, we present systems-level methods for *in vivo* flux quantification and systematically determine the direct sources and interconversion fluxes of the most important circulating nutrients. By direct source, we mean the circulating precursor that is chemically converted into the metabolic product of interest without going through other circulating nutrients. We further trace circulating nutrients into the TCA cycle of diverse tissues, revealing tissue fuel preferences. By conducting these analyses for both fasted and fed mice on either standard carbohydrate-rich lab chow (carbohydrate diet, CD) or a ketogenic diet (KD), we provide a systems-level quantitative view of mammalian metabolic activity across divergent diets. The resulting data reveal fundamental features

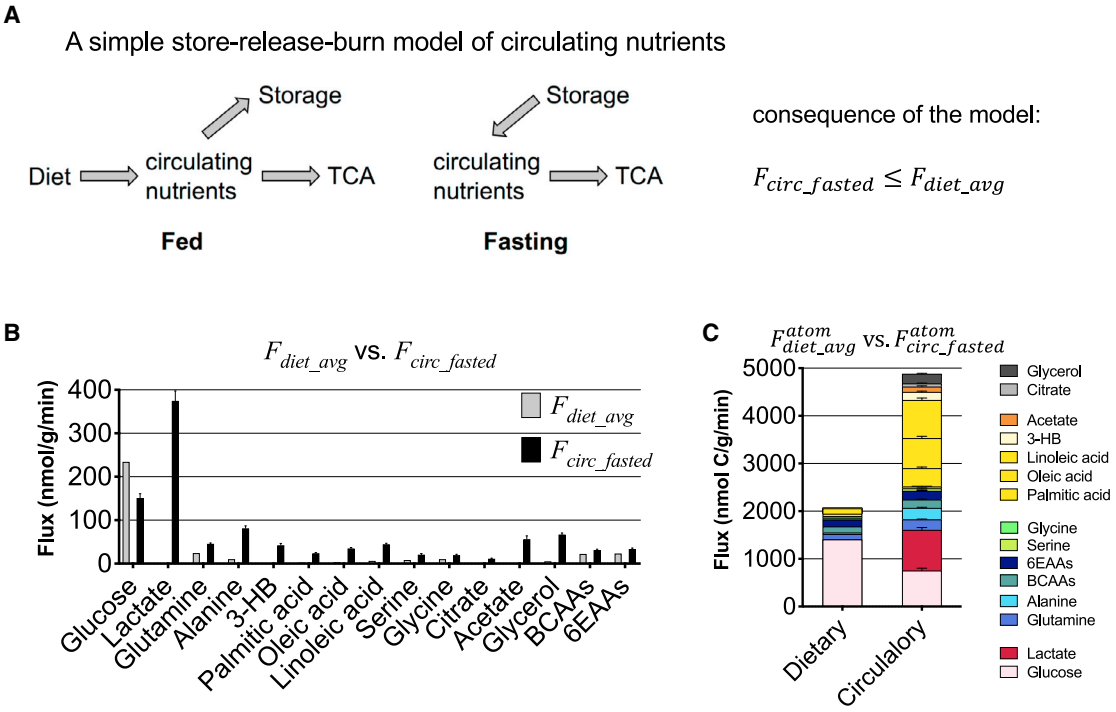

Figure 1. Circulatory Turnover Flux Markedly Exceeds Dietary Flux, Indicating Active Nutrient Cycling

Data are from 8-h fasted mice on carbohydrate diet.

(A) Hypothetical store-release-burn model. In fed state, circulating nutrients originate from the diet and go to either storage or tissue energy generation. In fasted state, circulating nutrients come from the storage and are consumed solely for tissue energy generation. For a nutrient that follows this model, in fasted state, its circulatory turnover flux is less than its average dietary intake flux averaged over a diurnal cycle. Data in (B) and (C) contradict this conclusion, indicating active nutrient cycling in the fasted state.

(B) Comparison between average dietary flux and fasted circulatory turnover flux for specific metabolites. See Table S2 for values of fluxes and n.

(C) Comparison between the average dietary flux and fasted circulatory turnover flux, here shown as stacked bars. In (B), the flux units are moles molecules. In (C), they are moles carbon. See Table S2 for values.

Data are shown as mean ± SEM.

of metabolism. Specific examples include glycerol standing out among major circulating metabolites in not being a direct TCA fuel, carbohydrate (i.e., glucose and lactate) being the main brain fuel even on KD, and heart being unique among organs in not burning circulating amino acids. More generally, we find that tissues have strong nutrient preferences that are maintained across feeding and fasting, and that major circulating nutrient cycles persist across physiological states and diets.

RESULTS

Comparison of Dietary Flux and Circulatory Flux

Consider the simple store-release-burn model shown in Figure 1A. In this hypothetical model, tissues are fed by dietary nutrients (e.g., glucose, amino acids), either directly or after their storage (e.g., in glycogen, protein). Define F_{diet} as dietary intake rate of a particular nutrient (units of nmol/min/g, dividing the intake rate by the mouse weight in grams); F_{circ} as the rate of disappearance of the nutrient or other metabolite from the bloodstream due to tissue consumption, which at pseudo-steady state is equivalent to its rate of appearance in the bloodstream from either diet or tissue excretion (STAR Methods) (Hui et al., 2017; Wolfe and Chinkes, 2005); and F_{burn} as the terminal clearance of the circulating nutrient, typically via burning into CO_2 in the TCA cycle. Each of these parameters can be determined during the fed state, fasted state, or as an average rate throughout the day. Ultimately, over a diurnal cycle, organisms maintain metabolic pseudo-steady state, and hence $F_{diet\_avg} = F_{burn\_avg}$. Moreover, in the store-release-burn model, in the fasted state, nutrients taken up from the bloodstream are burned to generate energy and not stored, and hence $F_{circ\_fasted} = F_{burn\_fasted}$. Because energy expenditure and thus nutrient burning is typically higher during feeding than fasting, $F_{circ\_fasted} = F_{burn\_fasted} \leq F_{burn\_avg} = F_{diet\_avg}$. Thus, in the store-release-burn model, $F_{circ\_fasted} \leq F_{diet\_avg}$.

The features of the hypothetical store-release-burn model can be compared to experimental flux data, to assess whether metabolism largely follows this logic or operates in a fundamentally different way. In previous work, we identified the circulating metabolites in mice that carry an F_{circ} greater than 10% of the glucose F_{circ} (Hui et al., 2017). Here, in addition to these 13 top circulating metabolites, for comprehensiveness, we also include two other groups of metabolites, the three branched-chain amino acids and six other essential amino acids (EAAs), which were infused together in uniformly ^{13}C-labeled form. Pyruvate was not included, as it is in rapid exchange with lactate and yet much less abundant

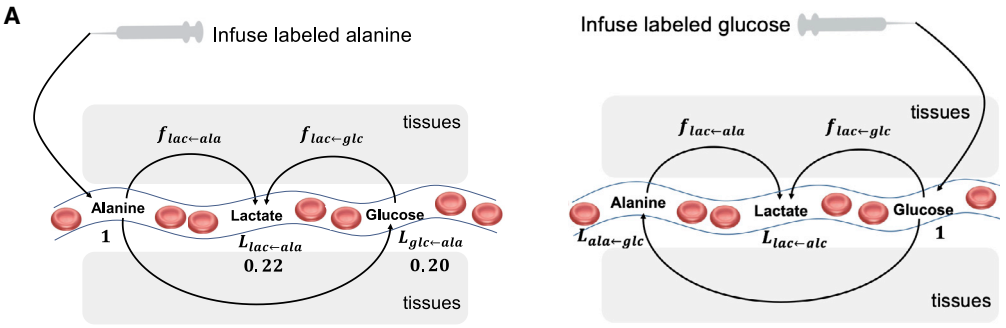

$$f_{lac\leftarrow ala} + f_{lac\leftarrow glc} \cdot L_{glc\leftarrow ala} = L_{lac\leftarrow ala}$$

$$f_{lac\leftarrow glc} + f_{lac\leftarrow ala} \cdot L_{ala\leftarrow glc} = L_{lac\leftarrow glc}$$

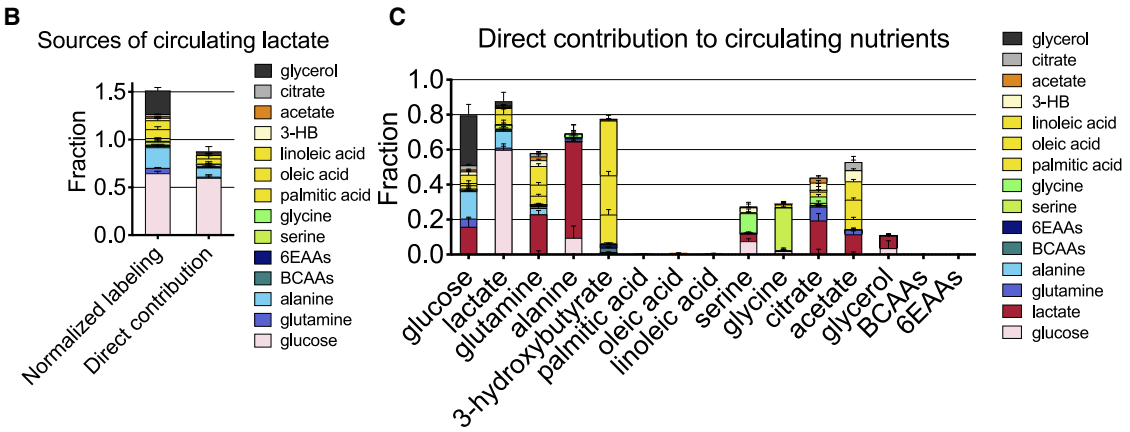

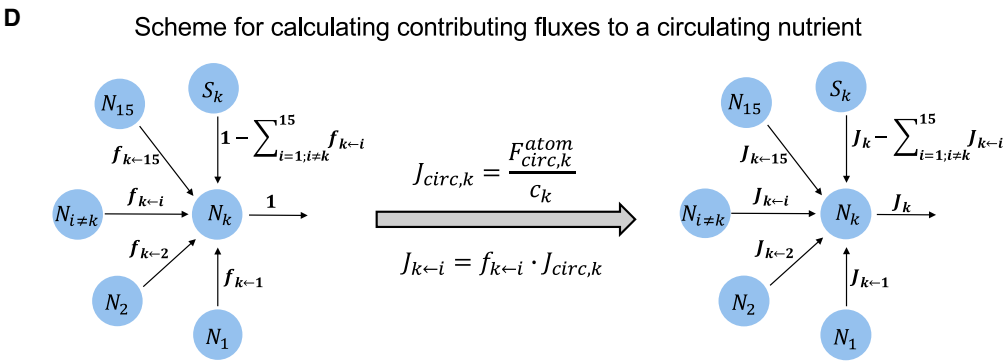

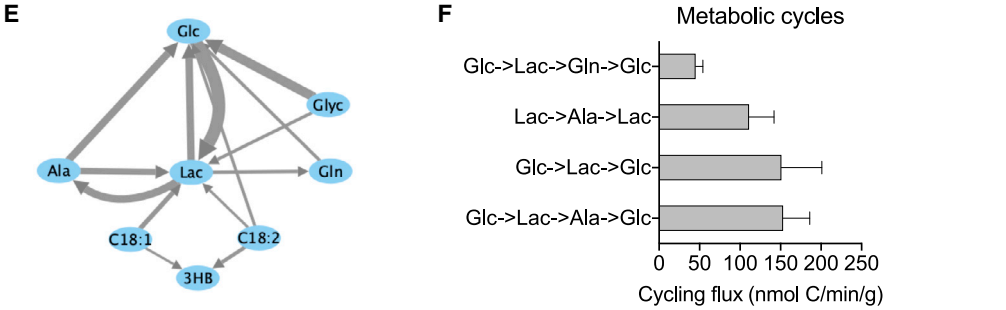

(legend on next page)

in the bloodstream (Romijn et al., 1994). To achieve minimal perturbation to the system and at the same time obtain reliable labeling measurements (including for downstream metabolites), we selected an infusion rate such that the final enrichment of tracer in serum is in the range of 10%–15% (for tracer solution concentrations and volumetric infusion rates, see Table S1). Monitoring of level of both serum metabolites and insulin confirmed the minimally perturbative nature of our infusions (Figure S1).

Consistent with the store-release-burn model, glucose and the EAAs show a pattern where $F_{circ\_fasted} \approx F_{diet\_avg}$ (Figure 1B; Table S2). Most of circulatory metabolic flux, however, resides in nutrients for which $F_{circ\_fasted} >> F_{diet\_avg}$: lactate, glutamine, fatty acids, glycerol, and acetate (Figure 1B; Table S2). Thus, metabolism is not primarily organized around storing, releasing, and burning dietary nutrients. Instead, interconversion between dietary nutrients and other circulating metabolic intermediates plays a large role.

Alternative Measure of Fluxes

In contrast to fluxes measured in units of mole nutrient, to better reflect overall contributions of nutrients to carbon metabolism, in the rest of the paper we report flux in units of mole carbon, such that two lactate are equivalent to one glucose and one-third of a C18 fatty acid. Thus, rather than reporting F_{circ}, which uses mass spectrometry to measure any loss of fully labeled infused tracer (even if some of the labeled tracer atoms remain), we report F_{circ}^{atom}, which we define as clearance of the labeled tracer atoms from the circulation (STAR Methods). F_{circ}^{atom} better aligns with classical radioactive tracer studies and facilitates certain downstream calculations (Wolfe and Chinkes, 2005). With the uniform units of nmol carbon/min/g for each nutrient, we can sum up the dietary fluxes and the circulatory turnover fluxes for an overall comparison (Figure 1C; Table S2). In the CD, dietary influx is dominated by glucose from carbohydrate. Yet lactate, free fatty acids, glycerol, and amino acids also have high circulatory turnover flux. The substantial circulatory turnover flux of nutrients other than glucose reflects widespread interconversion between dietary nutrients, circulating nutrients, and internal nutrient stores like protein and triglycerides.

Determining the Direct Sources of Circulating Metabolites

To determine the interconversion between dietary nutrients and circulating nutrients, we next aimed to quantify contributions of dietary nutrients to other circulating metabolites, and back again (in the case of metabolic cycles). To this end, for any circulating metabolite X, we wanted to figure out how much it contributes to any other circulating metabolite Y. The experimental approach is to infuse at a minimally perturbative rate uniformly ^{13}C-labeled X and measure the pseudo-steady-state labeling of Y. Specifically, upon infusion of X, we define the normalized labeling of Y ($L_{Y\leftarrow X}$) as fraction of labeled carbon atoms in serum Y relative to that of serum X (STAR Methods). For example, by infusing uniformly ^{13}C-alanine and measuring labeling of circulating alanine and lactate, we can determine $L_{lac\leftarrow ala}$.

This measure of labeling, however, cannot be taken as the direct contribution from alanine to lactate because the infused alanine may label lactate either directly or indirectly via other circulating metabolites (Figure 2A). For example, alanine might first be taken into one tissue, converted into glucose, and excreted into the circulation, and then the circulating glucose might be converted into circulating lactate. Thus, in alanine infusion, the labeling of lactate (L_{lac}) is the sum of the direct contribution from alanine to lactate ($f_{lac\leftarrow ala}$) weighted by the labeling of alanine (L_{ala}) and the indirect contribution through glucose, with the latter term equal to the direct contribution from glucose to lactate ($f_{lac\leftarrow glc}$) weighted by the labeling of glucose (L_{glc}). Dividing both sides of this equation by L_{ala}, we can express the equation in terms of normalized labeling (first equation in Figure 2A). The values of the normalized labeling are shown in the figure. Both direct contributions ($f_{lac\leftarrow ala}$ and $f_{lac\leftarrow glc}$) can be determined by separately infusing labeled alanine and labeled glucose and measuring the labeling of all three metabolites (lactate, alanine, and glucose) in both experiments.

This scheme can be extended to calculate the direct contribution from any circulating metabolite to any other circulating metabolite. To determine fully the inter-conversion between n circulating metabolites, we infuse each of them individually and measure their labeling in each infusion experiment. The resulting data form an $n \times n$ matrix (denoted as M) with rows corresponding to infused metabolites and columns to measured metabolites. The entry (i, j) of M is the normalized labeling of metabolite j by metabolite i. The diagonal entries of the matrix represent the normalized labeling of the infused metabolite itself and are 1 by the definition of normalized labeling. Experimental data for the 15 circulating metabolites studied here (the 13 highest flux individual metabolites + the 2 EAA mixtures) are shown in Table S3.

The direct contribution to circulating metabolite k from the other 14 circulating metabolites is given by a system of 14 linear equations:

$$M_k \cdot \begin{pmatrix} f_{k\leftarrow glc} \\ f_{k\leftarrow ala} \\ \vdots \\ f_{k\leftarrow 6EAAs} \end{pmatrix} = \begin{pmatrix} L_{k\leftarrow glc} \\ L_{k\leftarrow ala} \\ \vdots \\ L_{k\leftarrow 6EAAs} \end{pmatrix} \quad \text{(Equation 1)}$$

Figure 2. Comprehensive Tracer Studies Enable Determination of Direct Sources and Interconversion Fluxes of Circulating Metabolites

Data are for 8-h fasted mice on CD.

(A) Example of calculating the direct contributions from two circulating metabolites (alanine, glucose) to a third metabolite (lactate). This requires infusion separately of alanine and glucose. Each infusion experiment yields an isotope balance equation. Together, the two equations from the two infusions determine the two direct contributions.

(B) Comparison between the normalized labeling of lactate (calculated separately from each infusion) and the direct contributions to lactate.

(C) Direct contributions to each of 15 circulating metabolites from the other 14. See Table S3 for normalized labeling data and Table S4 for the direct contribution values.

(D) Scheme for calculating absolute contributing fluxes from the relative direct contributions.

(E) Circulating nutrient interconversion fluxes. Edge widths are proportional to log-transformed flux values. Shown are fluxes > 30 nmol C/min/g.

(F) Metabolic cycles with flux > 40 nmol C/min/g.

Data are shown as mean ± SEM.

M_k is the 14×14 submatrix of M with both the row and column corresponding to k removed, L is the column vector of the normalized labeling data from the isotope infusion experiments (mathematically, L is the *k-th* column of M with the *k-th* entry removed), and f is the length 14 column vector of direct contributions. While Equation 1 can be solved algebraically, to avoid negative values due to measurement errors, we use an optimization procedure to obtain the direct contributions (STAR Methods). Application of this procedure to lactate revealed that infusions of glucose, alanine, and other amino acids label lactate, but glucose is the predominant direct contributor: the amino acids are first converted to circulating glucose by gluconeogenesis and then the resulting labeled glucose makes lactate (Figure 2B). This discrepancy emphasizes the importance of determining direct contributions for elucidating the *in vivo* operation of metabolism.

Circulating Metabolite Sources

Equation 1 can be applied to each of the 15 nutrients to determine its direct contributions from the other 14 nutrients. The comprehensive direct contribution analysis in 8-h fasted mice reveals fundamental aspects of metabolism (Figure 2C; Table S4). Circulating glucose, lactate, alanine, and 3-hydroxybutyrate (3HB) come mainly from other circulating metabolites, as the sum of the circulating metabolite contributions is almost 1. In contrast, the circulating metabolite contributions to fatty acids and EAAs are negligible, reflecting their production instead by hydrolysis of triglycerides and protein. Circulating glucose is made from a roughly equal balance of lactate, alanine, and glycerol. Glucose is the dominant precursor of lactate, and lactate the main source of alanine. Circulating glycerol is made from both glucose and lactate, but mainly comes from stored triglycerides. Acetate is produced roughly equally from circulating metabolites and other sources (e.g., the microbiome, protein deacetylation). Despite recent evidence that glucose catabolism can make acetate (Liu et al., 2018), the predominant circulatory precursors to acetate are fatty acids.

Absolute Fluxes between Circulating Metabolites

The direct contribution analysis reveals the existence of futile metabolic cycles. For example, consistent with the Cori cycle, there is direct contribution from circulating lactate to circulating glucose, and vice versa (Figure 2C). While cycles can be identified from the direct contributions, to quantify the magnitude of the cycles, it is necessary to know the absolute fluxes between circulating metabolites. We denote the flux from circulating metabolite i to metabolite k as $J_{k\leftarrow i}$. Despite decades of research into metabolic cycles, a general method for determining such absolute fluxes has been lacking. Intuitively, the flux from i to k should reflect how fast circulating k is being produced (conceptually, F_{circ_k}) multiplied by the fraction of k coming from i ($f_{k\leftarrow i}$). The challenge is that F_{circ} (and equivalently classical measurements of R_a) actually measure dilution of the infused isotope-labeled metabolite in the bloodstream by incoming flux from diet or synthesis. If the incoming flux from synthesis is in part labeled (due to metabolic cycling), the absolute magnitude of the flux will be underestimated.

We developed an algorithm that uses the comprehensive interconversion data (i.e., the direct contributions between metabolites in Figure 2C and Table S4) to calculate a conversion factor (denoted as c_k) that relates the isotope measured $F^{atom}_{circ,k}$ and the absolute circulatory flux through that metabolite ($J_{circ,k}$), and accordingly can be used to determine the absolute circulatory fluxes. Absolute fluxes connecting circulating metabolites can then be determined by multiplying $J_{circ,k}$ by the direct contribution values (Figure 2D). Details of the algorithm can be found in Methods S1. The biggest absolute fluxes are glucose to lactate and lactate, alanine, and glycerol to glucose (Figure 2E).

Cycling of Circulating Nutrients

We define the magnitude of a metabolic cycle among nutrients as the minimum of the inter-converting fluxes between the nutrients, $J^{cycle}_{ik\cdots n} = \min(J_{i\leftarrow k}, \cdots, J_{n\leftarrow i})$. Figure 2F shows all metabolic cycles between circulating metabolites with flux greater than 40 nmol carbon/min/g (about 5% of the glucose F^{atom}_{circ}). This analysis identified the three highest flux metabolic cycles: glucose-lactate-glucose, lactate-alanine-lactate, and glucose-lactate-alanine-glucose (Figure 2F). This latter pathway is particularly interesting, reflecting that lactate (not glucose) is the predominant source of circulating alanine, and that alanine is co-equal with lactate as a contributor to gluconeogenesis, despite having much lower F^{atom}_{circ}. The analysis also identified a previously unrecognized metabolic cycle between circulating glucose, lactate, and glutamine, reflecting circulating lactate feeding the TCA cycle and circulating glutamine being produced from the TCA cycle and used as a gluconeogenesis substrate.

Persistence of the Metabolic Cycling in Fed Mice

We have so far focused on carbohydrate-diet mice fasted for 8 h (9 a.m. to 5 p.m., when they sleep and food intake is typically low). Over this duration, the respiratory exchange ratio (RER) drops from above 0.9 (reflecting mainly carbohydrate burning) to less than 0.8 (reflecting mainly fat burning) (Figure 3A). As expected, refeeding increases the RER consistent with resumption of carbohydrate burning (Figure 3A). Despite the strong change in RER, comprehensive circulatory turnover flux measurement revealed strikingly similar fluxes between fasted and refed mice, with the exception of much higher value for glucose in the fed state, reflecting glucose influx from the meal (Figure 3B; Table S2). The persistent lactate and fatty acid fluxes suggest continued Cori cycling and triglyceride cycling in the fed state.

We then proceeded to analyze direct contributions to circulating metabolites in the fed state. For many metabolites, including lactate, alanine, and glutamine, their sources were nearly unaltered. For others, including glucose, serine, and acetate, the fraction produced from circulating metabolites fell with feeding, reflecting their coming instead from the diet or, in the case of acetate, the gut microbiome (Figure 3C; Tables S3 and S4). Analysis of absolute fluxes connecting circulating metabolites revealed no substantial new fluxes in the fed state. Metabolic cycling involving glucose, lactate, alanine, and glutamine was, however, persistent (Figures 3D and 3E).

Measuring Direct TCA Cycle Contributions

A primary function of circulating metabolites is to support tissue energy production, which occurs primarily through the TCA cycle. We next aimed to determine the direct contribution of any circulating metabolite X to the TCA cycle of different tissues.

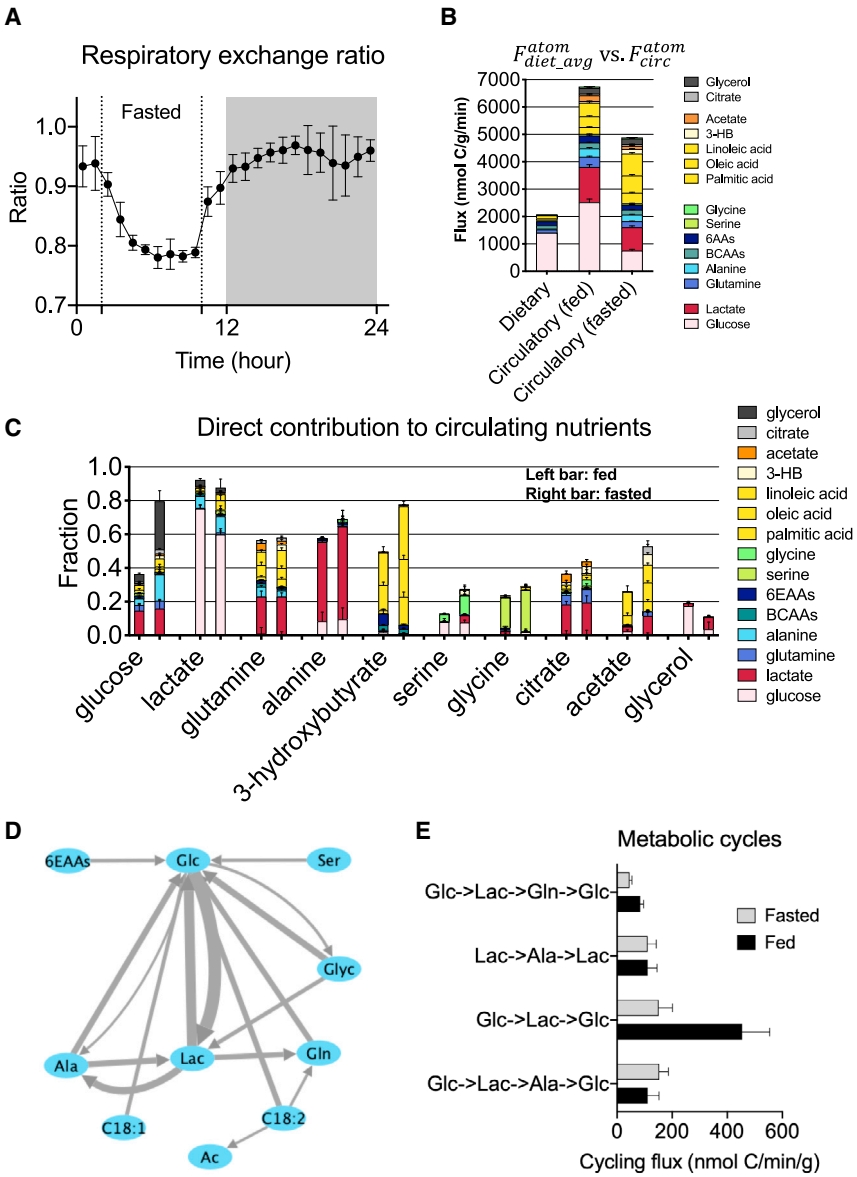

Figure 3. Metabolite Interconversion Fluxes Are Similar between Fed and Fasted Mice

Data are for 8-h fasted mice and 3-h refed mice on CD.

(A) Respiratory exchange ratio during a diurnal cycle (n = 5). Shaded area indicates the dark period. Mice were 8-h fasted during the light period.

(B) Dietary flux versus circulatory turnover flux in fed and fasted mice. See Table S2 for flux values and n.

(C) Direct contributions to circulating metabolites in both fed and fasted mice. For each metabolite, the left bar is fed state and right bar is fasted. See Table S3 for normalized labeling and Table S4 for direct contribution values.

(D) Circulating nutrient interconversion fluxes in fed mice. Edge widths are proportional to log-transformed flux values. Shown are fluxes > 30 nmol C/min/g.

(E) Top metabolic cycles in fed and fasted mice. Data are shown as mean ± SEM.

The experimental approach is to infuse uniformly ^{13}C-labeled *X* and measure tissue succinate and malate labeling. These two TCA intermediates are chosen for their higher concentration in tissues than in serum (Figure S1), enabling robust tissue-specific measurements. We define the normalized TCA labeling in tissue *i* from circulating metabolite *X* ($L_{TCA_i \leftarrow X}$) as the fraction of labeled carbon atoms in tissue malate or succinate relative to that of *X* in serum.

Due to the interconversion of circulating nutrients, the normalized TCA labeling of *X* may exceed its direct contribution, with *X* instead feeding the TCA cycle via other circulating metabolites (Figure 4A). For example, both glucose and glycerol infusions label TCA intermediates in most tissues (Figure 4B), but such labeling may occur indirectly via circulating lactate (Hui et al., 2017). The measured TCA labeling reflects the weighted sum of the direct and indirect routes from the infused tracer to the tissue TCA. For example, in Figure 4A, the measured TCA labeling from tracer *X* ($L_{TCA_i \leftarrow X}$) can be expressed in terms of the normalized labeling of *Y* ($L_{Y \leftarrow X}$) and *Z* ($L_{Z \leftarrow X}$) and the three direct contributions to TCA from *X*, *Y*, and *Z* (denoted as $f_{TCA_i \leftarrow X}$, $f_{TCA_i \leftarrow Y}$, and $f_{TCA_i \leftarrow Z}$, respectively). To determine all the three direct contributions in this example, we also need to infuse the other two nutrients and measure the labeling of both tissue malate and the other two nutrients in serum. The resulting three equations can then be used to solve for the three unknowns.

We generalized this scheme to determine the direct TCA contributions of the 13 high flux circulating metabolites plus the two amino acid mixtures. To this end, in addition to measuring the circulating metabolite interconversion matrix *M*, we also measured malate and succinate labeling from each of the 15 tracers across 11 tissues (data shown in Table S3 and Figure S2). For each tissue, the direct TCA contributions ($f_{TCA_i \leftarrow X}$) are determined by solving 15 linear equations:

$$M \cdot \begin{pmatrix} f_{TCA_i \leftarrow glc} \\ f_{TCA_i \leftarrow lac} \\ \vdots \\ f_{TCA_i \leftarrow 6EAAs} \end{pmatrix} = \begin{pmatrix} L_{TCA_i \leftarrow glc} \\ L_{TCA_i \leftarrow lac} \\ \vdots \\ L_{TCA_i \leftarrow 6EAAs} \end{pmatrix} \quad \text{(Equation 2)}$$

As in the case of calculating direct contributions between circulating nutrients, to avoid negative values due to measurement errors, we use an optimization procedure to obtain the direct contributions (STAR Methods). In the case of glucose and glycerol, direct TCA contributions are much lower than measured TCA labeling, emphasizing the capacity for this quantitative analysis to unveil metabolic fundamentals that are normally masked by interconversion among circulating nutrients (Figure 4B).

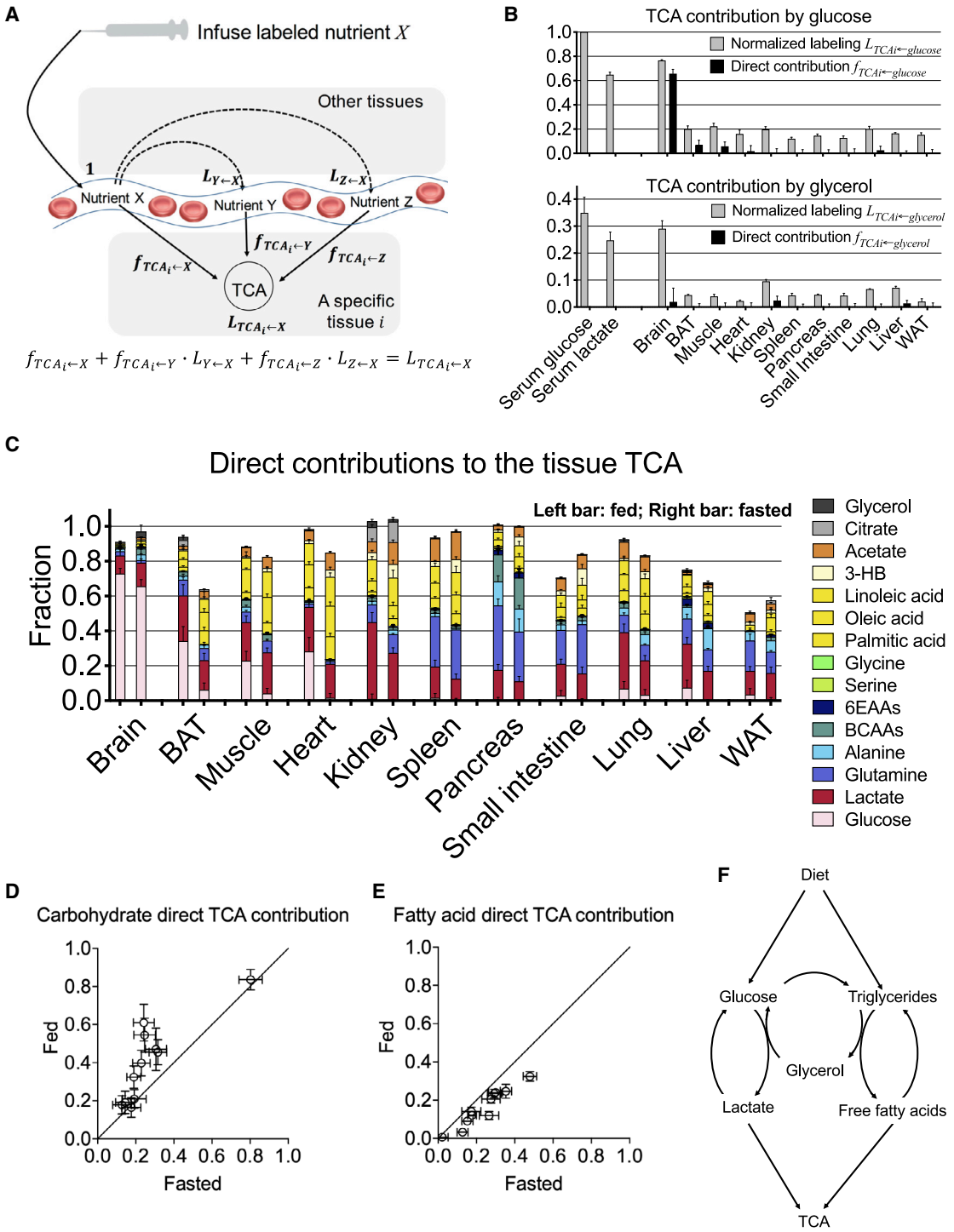

Figure 4. Comprehensive Tracer Studies Enable Determination of Direct Sources of Tissue TCA Metabolites

Data are for 8-h fasted mice and 3-h refed mice on CD.

(A) Example of direct and indirect routes from the infused tracer to tissue TCA cycle. The labeling of the tissue TCA upon labeled *X* infusion can come directly from *X* or indirectly via circulating *Y* or *Z*, as codified in the isotope-balance equation. Infusions of *Y* and *Z* yield analogous equations that are needed to solve for the three direct contributions.

(B) Glucose and glycerol label TCA intermediates indirectly, via other circulating metabolites. Comparison between the normalized labeling and direct contribution of glucose (upper panel) and glycerol (lower panel) to tissue malate shows higher labeling than direct contribution.

(legend continued on next page)

TCA Fuel Choices across Tissues

The tissue-specific direct TCA contributions provide a systems-level perspective of fuel utilization in both 8-h fasted and refed mice (Figure 4C; Table S5). The same trends are obtained using either malate or succinate labeling as the readout, supporting the robustness of the results (Figure S3). Brain is unique in mainly using glucose in both the fed and fasted states. In contrast to literature suggesting that the heart is an omnivore (Bing et al., 1954; Drake et al., 2012), cardiac muscle stands out for barely using circulating amino acids as fuels, preferentially consuming fatty acids. Kidney is unique in burning circulating citrate (Jang et al., 2019). Pancreas shows the greatest use of amino acids.

Consistent with the comprehensiveness of our analysis, in most tissues, the measured direct contributions almost add up to 1, reflecting a nearly comprehensive accounting for TCA carbon inputs. Notable exceptions are adipose and liver, where the missing carbon likely comes from burning of internal nutrient stores. In the fed-state small intestine and liver, the missing contribution may also include input from diet prior to mixing of incoming nutrients with the systemic circulation.

In general, tissues differed markedly in their metabolic preferences and maintained these preferences across the fed and fasted states. This manifests as a strong correlation between fasted and fed tissue carbohydrate (glucose/lactate) and fat usage (Figures 4D and 4E). In addition, there is a shift toward a greater carbohydrate contribution in feeding, and fat contribution in fasting (Figures 4D and 4E), with brown adipose and muscle being particularly responsive (Figure 4C).

The analysis also reveals which circulating metabolites directly drive TCA metabolism, with lactate, fatty acids, and (to a lesser extent) acetate serving as major contributors in nearly all tissues (Figure 4C). Glucose is the dominant precursor of circulating lactate (Figure 3C), and accordingly the origin of much TCA carbon, but itself contributes directly to TCA in only selected instances. Similarly, glycerol carries substantial circulatory flux and its infusion labels TCA in most tissues (Figure 4B), but it makes essentially no direct contribution (Figure 4C). Instead of being burned in TCA, glycerol is a dedicated gluconeogenic precursor (Figure 2C).

Together, the circulatory turnover flux, metabolite interconversion, and TCA contribution data support a model in which circulating glucose is constantly being interconverted with circulating lactate, and free fatty acids are constantly being released from and stored in triglycerides, with the bulk of energy being generated by tissue uptake and burning of lactate and free fatty acids, rather than glucose or triglycerides directly (Figure 4F).

Persistence of the Metabolic Cycling in Mice on Ketogenic Diet

Mammals cannot synthesize certain amino acids and fatty acids, and hence these are essential dietary components. Given adequate supply of these essential nutrients, mammals can survive on nearly pure carbohydrate or pure fat as the dominant caloric input. Standard lab chow, like a modern human diet high in bread or rice, provides most calories as carbohydrate. An opposite extreme is KD, which is mainly fat with minimal carbohydrate (25-fold less carbs than standard lab chow; Table S2). KD has been successfully used for almost a century as a treatment for refractory epilepsy (Barañano and Hartman, 2008; D'Andrea-Meira et al., 2019; Lima et al., 2014). More recently, KD is attracting interest for its ability to ameliorate type 2 diabetes (McKenzie et al., 2017) and even slow the progression of certain cancers (Allen et al., 2014; Hopkins et al., 2018; Lussier et al., 2016; Mavropoulos et al., 2009; Otto et al., 2008).

To examine how a radical change of diet affects metabolism, we performed both classical metabolic phenotyping (Figure S4) and circulatory flux analyses on mice adapted to a KD. Ketosis was confirmed with the elevated serum 3HB level on the KD (Figure S4). Consistent with literature, KD slightly decreased body weight and increased whole-body oxygen consumption and energy expenditure (Jornayvaz et al., 2010; Kennedy et al., 2007; Pissios et al., 2013). Despite the dietary inputs being almost completely different (Figure 5A; Table S2), F_{circ}^{atom} values were similar to standard CD (Figure 5B; Table S2). This supports the model in which chronic glucose-lactate cycling and triglyceride cycling render internal metabolic activity robust to changing dietary inputs.

To explore this concept further, we infused nine tracers (Figure S5; Table S6) to determine their interconversions and TCA inputs in KD (Figure 5C; Table S4). The infusion rate for glucose was decreased 4-fold to avoid perturbing metabolism or inducing insulin (Table S1; Figure S1). Alanine disappeared as a major gluconeogenic precursor in the KD, while glycerol emerged as a direct lactate precursor. Despite these shifts, the primary sources of each circulating metabolite remained the same. Moreover, while metabolic cycling involving alanine decreased, glucose-lactate cycling persisted, despite the near complete lack of dietary carbohydrate (Figure 5D). Thus, the nutrient cycling persists regardless of the dietary intake.

Pyruvate Cycling in Ketogenic Diet

Consistent with the low dietary intake of carbohydrates, the RER for mice on the KD remained low (~0.73) throughout the diurnal cycle (Figure 6A), indicating predominantly fatty acid burning. Assessment of TCA substrates revealed extensive fat and much decreased carbohydrate utilization in skeletal and cardiac muscle and brown adipose tissue (Figure 6B; Table S5). In addition, 3HB, which is derived from fatty acids (Figure 5C), emerged as a broadly important direct TCA input (Figure 6B). Interestingly, despite the paradigm that brain shifts from using glucose to

(C) Direct tissue TCA contributions for 15 circulating nutrients and 11 tissues. For each tissue, the left bar is fed state and right bar is fasted. See Table S3 for labeling data and Table S5 for direct TCA contribution values.
(D) Comparison of direct contribution from carbohydrates (the sum of direct contributions from glucose and lactate) to tissue TCA between fasted and fed mice.
(E) Comparison of direct contribution from fatty acids (the sum of direct contributions from palmitic acid, oleic acid, and linoleic acid) to tissue TCA between fasted and fed mice.
(F) Schematic of major carbohydrate and fatty acid fluxes: constant functioning of the glucose-lactate cycle and the triglyceride-glycerol-fatty acid cycle, with glycerol connecting the two, and lactate and free fatty acids the primary direct tissue TCA contributors.
Data are shown as mean ± SEM.

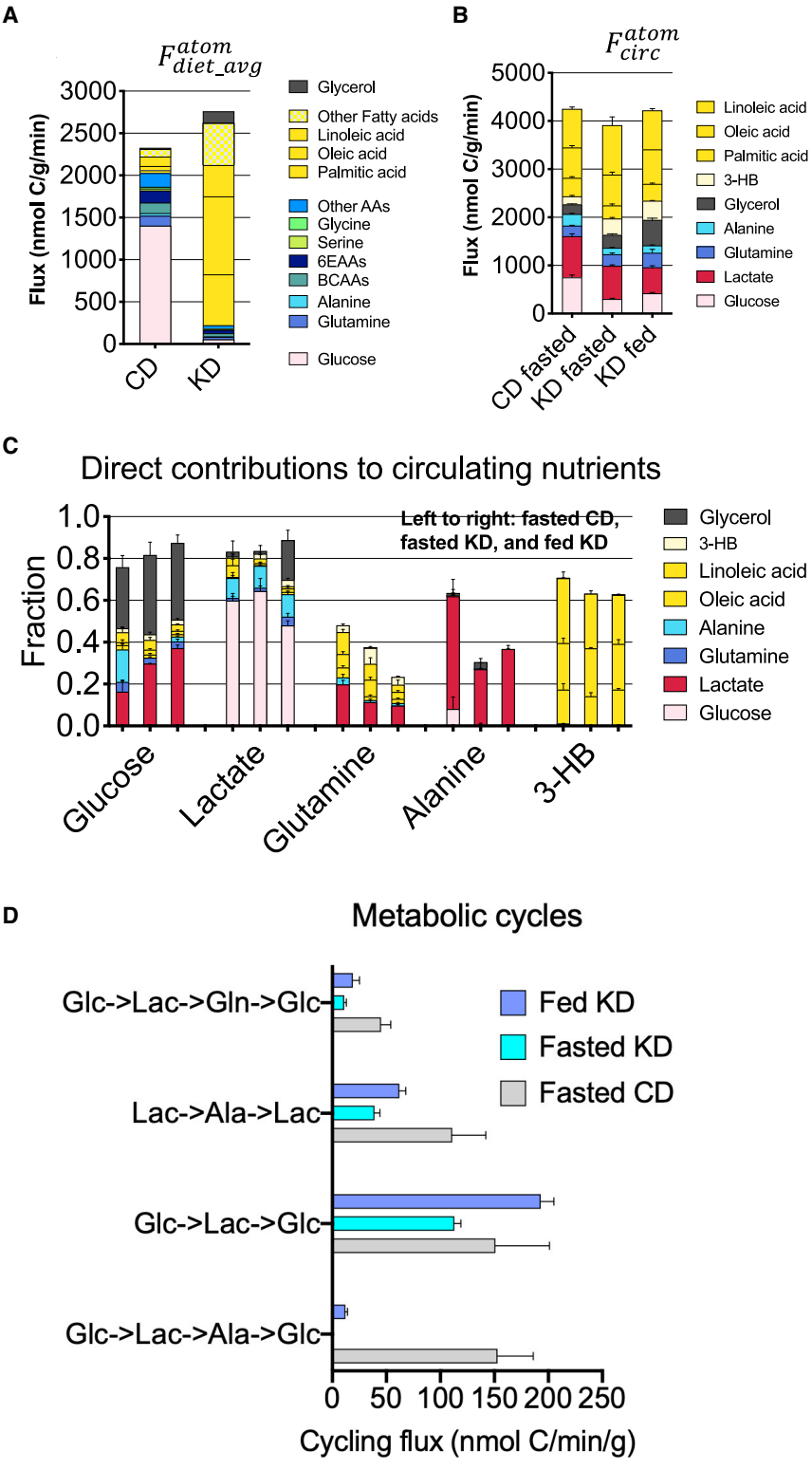

Figure 5. Persistent Circulatory Carbohydrate Fluxes on Ketogenic Diet

Data are for 8-h fasted CD mice and 8-h fasted and 3-h refed KD mice.

(A) Comparison of the dietary fluxes. See Table S2 for flux values and n.

(B) Comparison of the circulatory turnover fluxes. See Table S2 for flux values and n.

(C) Comparison of the direct contributions to circulating metabolites. For each metabolite, the left bar is fasted CD, middle bar is fasted KD, and right bar is fed KD. See Table S6 for labeling data and Table S4 for direct contribution values.

(D) Comparison of top metabolic cycles between the two diets.

Data are shown as mean ± SEM.

primarily using 3HB during ketosis (LaManna et al., 2009; Zhang et al., 2013), glucose remained the largest brain TCA substrate, with lactate also serving as a major contributor. Collectively, even on KD, more than 60% of brain TCA carbon still comes from carbohydrate (Figure 6C). Similarly, there was a substantial persistent lactate contribution to TCA cycle in many tissues, most notably kidney and liver (Figure 6C). Thus, analysis of TCA inputs revealed persistent carbohydrate metabolism in brain, kidney, and liver.

Carbohydrate can enter the TCA cycle through two routes: oxidation to acetyl-CoA by pyruvate dehydrogenase (PDH) or carboxylation to oxaloacetate. The former burns carbohydrate, while the latter generates four-carbon units that can remake glucose via gluconeogenesis. PDH removes C1 of lactate/pyruvate. Hence, [1-^{13}C]lactate infusion can be used to selectively trace TCA entry via pyruvate carboxylase (Figure 6D). Strikingly, on KD, the persistent carbohydrate TCA contribution in kidney and liver reflects strong pyruvate carboxylase activity. Such activity, which is a general feature of many tissues irrespective of diet (Figure 6E for KD; Figure S6 for CD), does not burn carbohydrate, but rather supports glucose-lactate cycling. Extensive pyruvate carboxylase activity in kidney and other non-hepatic organs implies that analysis of pyruvate cycling needs to consider the whole body, not solely liver metabolism (Burgess et al., 2015; Hasenour et al., 2015; Perry et al., 2016). The observed pyruvate carboxylase activity in non-gluconeogeneic organs may be important for providing TCA four-carbon units, which are required in catalytic amounts to enable TCA turning. Notably, the large carbohydrate contribution to brain TCA on KD is not associated with substantial pyruvate carboxylase activity, and instead reflects carbohydrate burning. Collectively, these observations support a model in which glucose-lactate cycling persists in KD, driven

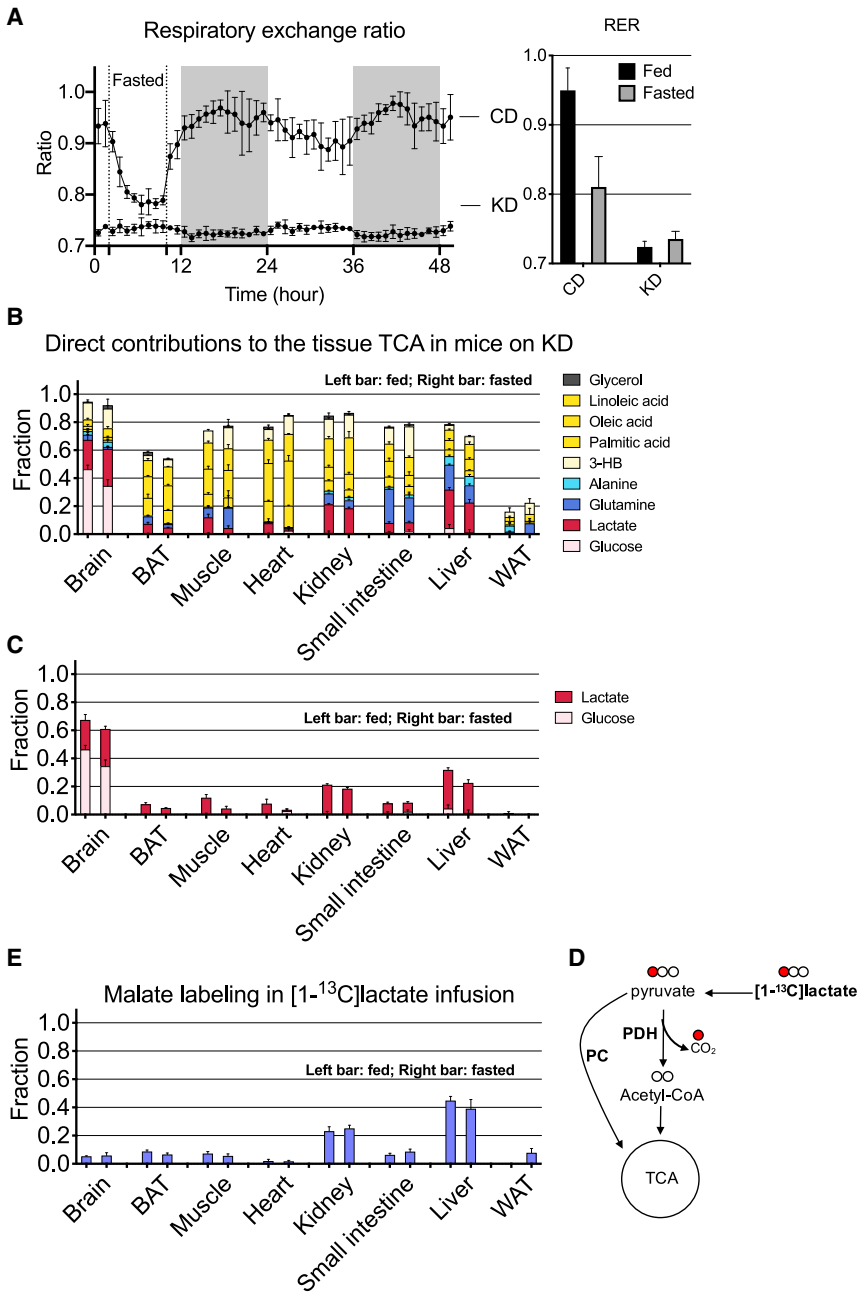

Figure 6. In Ketogenic Diet, Pyruvate Cycling Produces Carbohydrate Fluxes without Carbohydrate Burning

(A) Comparison of RER between mice on the high CD (n = 5) and the KD (n = 4). Shaded areas indicate the dark periods. Mice were fasted for 8 h in the first light period. Error bars are SDs.

(B) Direct contributions from 9 circulating metabolites to the TCA cycle in tissues of fasted mice and fed mice on the KD. See Table S6 for labeling data and Table S5 for direct TCA contribution values.

(C) Same data as in (B), but only the glucose and lactate data are shown.

(D) The labeled carbon of [1-^{13}C]lactate is lost in the PDH reaction, and hence labeling observed reflects TCA input via the PC pathway.

(E) Analogous to (C), with [1-^{13}C]lactate as the tracer.

Data are shown as mean ± SEM.

by lactate uptake into both liver and kidney TCA via pyruvate carboxylase to support gluconeogenesis, with carbohydrate burning via PDH turned off in all organs except for the brain.

DISCUSSION

Mammals are nourished by the food they eat. Food is initially converted into monomeric nutrients like glucose and amino acids. These nutrients can then be stored or interconverted. This processing ensures that the circulation carries a steady supply of appropriate nutrients to each tissue, despite varying dietary intake. To examine this processing comprehensively and quantitatively, we carried out isotope-tracer infusions for all high-flux circulating metabolites. Infusion rates were chosen to generate quantifiable labeling without substantially altering circulating metabolite concentrations or inducing insulin release. Using liquid chromatography-mass spectrometry (LC-MS), we measured experimentally the extent to which any given metabolite labels other circulating metabolites, as well as its tissue-specific TCA contributions.

The comprehensiveness of these experiments enables quantitative analyses that are not possible from studying any single nutrient in isolation. Specifically, the experimentally observed labeling from any given nutrient tracer reflects the sum of all routes linking the tracer to the measured metabolic product. Accordingly, the direct metabolic connections are clouded by interconversions among nutrients. Using our comprehensive measurements, through robust and readily implemented linear algebra analyses, we illuminate the direct metabolic connections and their quantitative magnitudes. In doing so, we provide fundamental reference data regarding *in vivo* metabolic activity and methods that can be applied across organisms, diets, and disease states.

Glycerol metabolism highlights the utility of determining direct contributions, rather than merely labeling. We find that glycerol is unique among high-flux circulating nutrients in not being catabolized into the TCA cycle in any tissue. This makes physiological sense. To survive prolonged starvation, mammals catabolize stored triglycerides, which yields fatty acids and glycerol. Because fatty acids cannot support gluconeogenesis, the resulting three-carbon units are precious and there is no sense in burning glycerol. Substantial flux flows directly from glycerol to glucose without passing through the TCA cycle. This result aligns

with genetic evidence that PEPCK deficiency does not impair glycerol-driven gluconeogenesis (van den Berghe, 1996). Importantly, however, a naive labeling measurement would show a clear TCA contribution from glycerol, due to its indirect TCA contributions via circulating glucose and lactate. Its special physiological role becomes clear from our systems-level analysis.

Direct contributions also provide a sharp picture of tissue TCA fuel preferences. Muscle and brown adipose tissue show strong responses to feeding, fluxing glucose carbon directly into their TCA cycle selectively in the fed state. This is consistent with the insulin-sensitive glucose uptake by these tissues (Kahn and Flier, 2000; Shulman, 2000; Townsend and Tseng, 2014; Trayhurn, 1995). In contrast, most other tissues show remarkably stable fuel preferences across feeding, fasting, and even KD. Lactate is unique in being a universal TCA substrate. Fat is also widely used, except in brain. Acetate is a relatively major contributor in many organs, but not brain or liver, where it is instead directed toward lipogenesis (Zhao et al., 2016). Amino acids are preferred fuels for the visceral organs, but not muscle.

Nutrient interconversion enables tissues to access their preferred fuels, even when dietary content changes. In the United States, roughly half of caloric intake is carbohydrates, one-third fat, and one-sixth protein (CDC, 2000). Mammals can thrive, however, eating either minimal fat or minimal carbohydrate (Hu et al., 2018; Simpson and Raubenheimer, 2012). Diets sufficiently low in both carbohydrate and protein are ketogenic: they lead to high circulating levels of ketone bodies, most importantly 3HB, made from fat by liver. Given that the brain does not effectively take up fatty acids, 3HB is widely assumed to be the major brain fuel during ketosis (LaManna et al., 2009; Zhang et al., 2013). Our analyses paint a different picture. 3HB contributes broadly to TCA, to a similar extent in brain, muscle, kidney, and intestine. In the brain, glucose and lactate, the two main forms of circulating carbohydrate, remain greater TCA contributors than 3HB. The continuous supply of carbohydrate to the brain, despite its near absence in the diet, is enabled by conversion of the glycerol moiety in dietary triglycerides into circulating glucose by the liver and kidney.

A key finding of our work is that such metabolic interconversions do not occur at a minimal rate, just sufficient for tissue demands. Instead, we observe rapid futile cycling, particularly for nutrients that are scarce in the diet. For example, in standard high-carbohydrate chow, we observe high circulatory turnover fluxes of fatty acids, with circulatory fatty acid and carbohydrate fluxes of similar magnitude. This reflects continuous triglyceride breakdown, release of fatty acids into the bloodstream, and their subsequent uptake and reincorporation into tissue fat. This cycling ensures a robust supply of fat and glycerol should demand arise (Newsholme et al., 1983). Strikingly, in KD, circulatory fatty acid fluxes are no higher than in the CD, and circulatory carbohydrate fluxes are only modestly lower. This reflects continuous synthesis of lactate from glucose and glucose from lactate. Alanine fluxes are, however, down, presumably due to lower dietary protein intake decreasing the need for nitrogen shuttling to the liver (Felig, 1973).

The relatively invariant circulatory fluxes of fatty acids, glycerol, lactate, and glucose across diets does not mean that the importance of these nutrients as fuels is steady. To maintain mass balance, mammals must burn what they eat. This divergence between nutrient cycling, which is relatively insensitive to diet, and nutrient burning, which changes with diet, is neatly captured by tracing positionally labeled lactate into the TCA cycle. In KD, lactate continues to enter the TCA cycle, especially in brain, liver, and kidney. In the brain, this entry is via PDH, reflecting the brain continuing to burn carbohydrate. In liver and kidney, however, entry is via pyruvate carboxylase, which does not destroy the three-carbon unit, but instead initiates its use for gluconeogenesis. Functionally, this makes sense. Persistent nutrient cycling ensures availability of the most important energy substrates to tissues irrespective of the physiological state. Tight regulation of burning ensures that limiting nutrients are saved for the tissues that need them most.

Overall, we lay out quantitative, systems-level methods for dissecting mammalian metabolism. The heart of these methods is mathematical integration of diverse tracer data to reveal direct connections both among circulating metabolites and between circulating metabolites and tissue TCA intermediates. Direct connections are not the only ones that matter functionally. For example, most lactate carbon originates from glucose. Accordingly, the minimal direct TCA contribution of glucose does not reflect a lack of glucose burning, but merely that circulating lactate is an intermediate in this process. In this way, direct contributions provide discrete measures of metabolic activity that can be used to advance quantitative understanding of metabolic physiology. Going forward, it will be important to relate these quantitative physiological measures both to underlying biochemical events and to the action of hormonal regulators that control metabolic health.

Limitations of the Study

Our analyses are based on average carbon labeling in different metabolites. The averaging is a form of coarse graining, a well-established strategy in the physical sciences for reducing complexity and thereby quantitatively capturing major system features (Kardar, 2007). Additional information is contained in the fraction of specific isotopic forms, which should be useful in future work for determining the fluxes of specific reactions within tissues (Antoniewicz, 2015; Dai and Locasale, 2017; Wiechert, 2001; Zamboni et al., 2009). One important example is differentiating TCA feeding via acetyl-CoA versus anaplerosis. Absent such differentiation, the TCA contributions reported here do not always correspond to tissue energy sources. For example, as shown by the [1-^{13}C]lactate tracing, for the liver and kidney, carbohydrates contribute to TCA mainly via pyruvate carboxylase. Thus, while lactate contributes much hepatic and renal TCA carbon, energy comes substantially from other substrates. These potentially include lipoproteins (Lambert et al., 2014; van der Veen et al., 2007) or macromolecules ingested via macropinocytosis (Swanson and Watts, 1995), in addition to the circulating monomeric nutrients explored here.

More generally, the present work is limited to two different diets in mice. While a valuable mammalian model, mice are small and devote a large fraction of energy to maintaining body heat. The extensive futile metabolic cycling observed here may have evolved in part to serve this function, and may be less in larger

mammals including humans. Studies of a broader range of diets and species, including clinical studies, are of great importance.

STAR★METHODS

Detailed methods are provided in the online version of this paper and include the following:

- KEY RESOURCES TABLE
- RESOURCE AVAILABILITY
  - Lead Contact
  - Materials Availability
  - Data and Code Availability
- EXPERIMENTAL MODEL AND SUBJECT DETAILS
- METHOD DETAILS
  - Metabolite Extraction of Serum
  - Metabolite Extraction of Tissue
  - Metabolite Measurement by LC-MS
  - Indirect Calorimetry
  - Insulin Measurement
- QUANTIFICATION AND STATISTICAL ANALYSIS
  - Calculation of Average Dietary Fluxes
  - Definition of F_{circ} and F_{circ}^{atom}
  - Definition of Normalized Labeling
  - Calculation of Direct Contributions with the Constraint of Non-negative Values
  - Quantification of Absolute Flux between Circulating Nutrients

SUPPLEMENTAL INFORMATION

Supplemental Information can be found online at https://doi.org/10.1016/j.cmet.2020.07.013.

ACKNOWLEDGMENTS

S.H. is supported by NIH grant R00DK117066. T.T. is supported by NIH grant 1F32DK118856-01A1. C.J. is a postdoctoral fellow of the American Diabetes Association (1-17-PDF-076). W.L. is supported by NIH grant CA211437. This work was supported by NIH Pioneer award 1DP1DK113643, the Paul G. Allen Family Foundation grant 0034665, and NIH grant P30 DK019525 to the University of Pennsylvania Diabetes Research Center (DRC), for both the Metabolomics and Rodent Phenotyping Cores. We thank members of the Rabinowitz lab and U Penn DRC for scientific discussions.

AUTHOR CONTRIBUTIONS

S.H., A.J.C., and J.D.R. designed the study. S.H. performed most experiments and data analysis in mice fed on high CD. A.J.C. performed most experiments and data analysis in mice fed on KD. X.Z. performed isotopic labeling measurement of acetate. L.Y. contributed to isotope tracing experiments in mice fed on KD. X.Z., X.L., C.B., Z.Z., C.J., and L.W. contributed to isotope tracing experiments in mice fed on high CD. S.H. and J.D.R. performed the flux modeling. L.W. and W.L. contributed to LC-MS analysis of metabolites. A.J.C., J.R., and J.B. contributed to metabolic measurements of mice. S.H., A.J.C., and J.D.R. wrote the manuscript. All authors discussed the results and commented on the manuscript.

DECLARATION OF INTERESTS

J.D.R. is a member of the Rutgers Cancer Institute of New Jersey and of the University of Pennsylvania Diabetes Research Center; a co-founder and stockholder in VL54, Sofro, and Raze Therapeutics; and advisor and stockholder in Agios Pharmaceuticals, Kadmon Pharmaceuticals, Bantam Pharmaceuticals, Colorado Research Partners, Rafael Pharmaceuticals, and L.E.A.F. Pharmaceuticals.

Received: February 4, 2020
Revised: April 6, 2020
Accepted: July 20, 2020
Published: August 12, 2020

REFERENCES

Allen, B.G., Bhatia, S.K., Anderson, C.M., Eichenberger-Gilmore, J.M., Sibenaller, Z.A., Mapuskar, K.A., Schoenfeld, J.D., Buatti, J.M., Spitz, D.R., and Fath, M.A. (2014). Ketogenic diets as an adjuvant cancer therapy: History and potential mechanism. Redox Biol. *2*, 963–970.

Antoniewicz, M.R. (2015). Methods and advances in metabolic flux analysis: a mini-review. J. Ind. Microbiol. Biotechnol. *42*, 317–325.

Barañano, K.W., and Hartman, A.L. (2008). The ketogenic diet: uses in epilepsy and other neurologic illnesses. Curr. Treat. Options Neurol. *10*, 410–419.

Bing, R.J., Siegel, A., Ungar, I., and Gilbert, M. (1954). Metabolism of the human heart. II. Studies on fat, ketone and amino acid metabolism. Am. J. Med. *16*, 504–515.

Burgess, S.C., Merritt, M.E., Jones, J.G., Browning, J.D., Sherry, A.D., and Malloy, C.R. (2015). Limitations of detection of anaplerosis and pyruvate cycling from metabolism of [1-(13)C] acetate. Nat. Med. *21*, 108–109.

CDC (2000). Intake of Calories and Selected Nutrients for the United States Population, 1999-2000 (Center for Disease Control and Prevention).

D'Andrea Meira, I., Romão, T.T., Pires do Prado, H.J., Krüger, L.T., Pires, M.E.P., and da Conceição, P.O. (2019). Ketogenic diet and epilepsy: what we know so far. Front. Neurosci. *13*, 5.

Dai, Z., and Locasale, J.W. (2017). Understanding metabolism with flux analysis: from theory to application. Metab. Eng. *43* (Pt B), 94–102.

Drake, K.J., Sidorov, V.Y., McGuinness, O.P., Wasserman, D.H., and Wikswo, J.P. (2012). Amino acids as metabolic substrates during cardiac ischemia. Exp. Biol. Med. (Maywood) *237*, 1369–1378.

Felig, P. (1973). The glucose-alanine cycle. Metabolism *22*, 179–207.

Frayn, K.N. (2009). Metabolic Regulation: A Human Perspective (John Wiley & Sons).

Hasenour, C.M., Wall, M.L., Ridley, D.E., Hughey, C.C., James, F.D., Wasserman, D.H., and Young, J.D. (2015). Mass spectrometry-based microassay of (2)H and (13)C plasma glucose labeling to quantify liver metabolic fluxes in vivo. Am. J. Physiol. Endocrinol. Metab. *309*, E191–E203.

Hopkins, B.D., Pauli, C., Du, X., Wang, D.G., Li, X., Wu, D., Amadiume, S.C., Goncalves, M.D., Hodakoski, C., Lundquist, M.R., et al. (2018). Suppression of insulin feedback enhances the efficacy of PI3K inhibitors. Nature *560*, 499–503.

Hu, S., Wang, L., Yang, D., Li, L., Togo, J., Wu, Y., Liu, Q., Li, B., Li, M., Wang, G., et al. (2018). Dietary fat, but not protein or carbohydrate, regulates energy intake and causes adiposity in mice. Cell Metab. *28*, 415–431.e4.

Hui, S., Ghergurovich, J.M., Morscher, R.J., Jang, C., Teng, X., Lu, W., Esparza, L.A., Reya, T., Le Zhan, Yanxiang Guo, J., et al. (2017). Glucose feeds the TCA cycle via circulating lactate. Nature *551*, 115–118.

Jang, C., Hui, S., Zeng, X., Cowan, A.J., Wang, L., Chen, L., Morscher, R.J., Reyes, J., Frezza, C., Hwang, H.Y., et al. (2019). Metabolite exchange between mammalian organs quantified in pigs. Cell Metab. *30*, 594–606.e3.

Jornayvaz, F.R., Jurczak, M.J., Lee, H.-Y., Birkenfeld, A.L., Frederick, D.W., Zhang, D., Zhang, X.-M., Samuel, V.T., and Shulman, G.I. (2010). A high-fat, ketogenic diet causes hepatic insulin resistance in mice, despite increasing energy expenditure and preventing weight gain. Am. J. Physiol. Endocrinol. Metab. *299*, E808–E815.

Kahn, B.B., and Flier, J.S. (2000). Obesity and insulin resistance. J. Clin. Invest. *106*, 473–481.

Kardar, M. (2007). Statistical Physics of Fields (Cambridge University Press).

Kennedy, A.R., Pissios, P., Otu, H., Roberson, R., Xue, B., Asakura, K., Furukawa, N., Marino, F.E., Liu, F.F., Kahn, B.B., et al. (2007). A high-fat, ketogenic diet induces a unique metabolic state in mice. Am. J. Physiol. Endocrinol. Metab. *292*, E1724–E1739.

LaManna, J.C., Salem, N., Puchowicz, M., Erokwu, B., Koppaka, S., Flask, C., and Lee, Z. (2009). Ketones suppress brain glucose consumption. In Oxygen Transport to Tissue XXX, P. Liss, P. Hansell, D.F. Bruley, and D.K. Harrison, eds. (Springer), pp. 301–306.

Lambert, J.E., Ramos-Roman, M.A., Browning, J.D., and Parks, E.J. (2014). Increased de novo lipogenesis is a distinct characteristic of individuals with nonalcoholic fatty liver disease. Gastroenterology *146*, 726–735.

Lima, P.A., Sampaio, L.P.B., and Damasceno, N.R.T. (2014). Neurobiochemical mechanisms of a ketogenic diet in refractory epilepsy. Clinics (São Paulo) *69*, 699–705.

Liu, X., Cooper, D.E., Cluntun, A.A., Warmoes, M.O., Zhao, S., Reid, M.A., Liu, J., Lund, P.J., Lopes, M., Garcia, B.A., et al. (2018). Acetate production from glucose and coupling to mitochondrial metabolism in mammals. Cell *175*, 502–513.e13.

Lussier, D.M., Woolf, E.C., Johnson, J.L., Brooks, K.S., Blattman, J.N., and Scheck, A.C. (2016). Enhanced immunity in a mouse model of malignant glioma is mediated by a therapeutic ketogenic diet. BMC Cancer *16*, 310.

Mavropoulos, J.C., Buschemeyer, W.C., 3rd, Tewari, A.K., Rokhfeld, D., Pollak, M., Zhao, Y., Febbo, P.G., Cohen, P., Hwang, D., Devi, G., et al. (2009). The effects of varying dietary carbohydrate and fat content on survival in a murine LNCaP prostate cancer xenograft model. Cancer Prev. Res. (Phila.) *2*, 557–565.

McKenzie, A.L., Hallberg, S.J., Creighton, B.C., Volk, B.M., Link, T.M., Abner, M.K., Glon, R.M., McCarter, J.P., Volek, J.S., and Phinney, S.D. (2017). A novel intervention including individualized nutritional recommendations reduces hemoglobin A1c level, medication use, and weight in type 2 diabetes. JMIR Diabetes *2*, e5.

Newsholme, E., and Leech, A. (2011). Functional Biochemistry in Health and Disease (John Wiley & Sons).

Newsholme, E.A., Arch, J.R., Brooks, B., and Surholt, B. (1983). The Role of Substrate Cycles in Metabolic Regulation (Portland Press Limited).

Otto, C., Kaemmerer, U., Illert, B., Muehling, B., Pfetzer, N., Wittig, R., Voelker, H.U., Thiede, A., and Coy, J.F. (2008). Growth of human gastric cancer cells in nude mice is delayed by a ketogenic diet supplemented with omega-3 fatty acids and medium-chain triglycerides. BMC Cancer *8*, 122.

Perry, R.J., Borders, C.B., Cline, G.W., Zhang, X.-M., Alves, T.C., Petersen, K.F., Rothman, D.L., Kibbey, R.G., and Shulman, G.I. (2016). Propionate increases hepatic pyruvate cycling and anaplerosis and alters mitochondrial metabolism. J. Biol. Chem. *291*, 12161–12170.

Pissios, P., Hong, S., Kennedy, A.R., Prasad, D., Liu, F.-F., and Maratos-Flier, E. (2013). Methionine and choline regulate the metabolic phenotype of a ketogenic diet. Mol. Metab. *2*, 306–313.

Reshef, L., Olswang, Y., Cassuto, H., Blum, B., Croniger, C.M., Kalhan, S.C., Tilghman, S.M., and Hanson, R.W. (2003). Glyceroneogenesis and the triglyceride/fatty acid cycle. J. Biol. Chem. *278*, 30413–30416.

Romijn, J.A., Chinkes, D.L., Schwarz, J.M., and Wolfe, R.R. (1994). Lactate-pyruvate interconversion in blood: implications for in vivo tracer studies. Am. J. Physiol. *266*, E334–E340.

Shulman, G.I. (2000). Cellular mechanisms of insulin resistance. J. Clin. Invest. *106*, 171–176.

Simpson, S.J., and Raubenheimer, D. (2012). The Nature of Nutrition: A Unifying Framework from Animal Adaptation to Human Obesity (Princeton University Press).

Swanson, J.A., and Watts, C. (1995). Macropinocytosis. Trends Cell Biol. *5*, 424–428.

Townsend, K.L., and Tseng, Y.-H. (2014). Brown fat fuel utilization and thermogenesis. Trends Endocrinol. Metab. *25*, 168–177.

Trayhurn, P. (1995). Fuel selection in brown adipose tissue. Proc. Nutr. Soc. *54*, 39–47.

van den Berghe, G. (1996). Disorders of gluconeogenesis. J. Inherit. Metab. Dis. *19*, 470–477.

van der Veen, J.N., Havinga, R., Bloks, V.W., Groen, A.K., and Kuipers, F. (2007). Cholesterol feeding strongly reduces hepatic VLDL-triglyceride production in mice lacking the liver X receptor alpha. J. Lipid Res. *48*, 337–347.

Wiechert, W. (2001). 13C metabolic flux analysis. Metab. Eng. *3*, 195–206.

Wolfe, R.R., and Chinkes, D.L. (2005). Isotope Tracers in Metabolic Research: Principles and Practice of Kinetic Analysis (John Wiley & Sons).

Zamboni, N., Fendt, S.-M., Rühl, M., and Sauer, U. (2009). (13)C-based metabolic flux analysis. Nat. Protoc. *4*, 878–892.

Zhang, Y., Kuang, Y., Xu, K., Harris, D., Lee, Z., LaManna, J., and Puchowicz, M.A. (2013). Ketosis proportionately spares glucose utilization in brain. J. Cereb. Blood Flow Metab. *33*, 1307–1311.

Zhao, S., Torres, A., Henry, R.A., Trefely, S., Wallace, M., Lee, J.V., Carrer, A., Sengupta, A., Campbell, S.L., Kuo, Y.M., et al. (2016). ATP-citrate lyase controls a glucose-to-acetate metabolic switch. Cell Rep. *17*, 1037–1052.

STAR★METHODS

KEY RESOURCES TABLE

REAGENT or RESOURCE	SOURCE	IDENTIFIER
Chemicals, Peptides, and Recombinant Proteins		
D-GLUCOSE (U-13C6, 99%)	Cambridge Isotope Laboratories	Cat# CLM-1396-PK
SODIUM L-LACTATE (13C3, 98%) 20% W/W in H2O	Cambridge Isotope Laboratories	Cat# CLM-1579-PK
SODIUM L-LACTATE (1-13C, 99%) 20% W/W in H2O	Cambridge Isotope Laboratories	Cat# CLM-1577-PK
L-GLUTAMINE (13C5, 99%)	Cambridge Isotope Laboratories	Cat# CLM-1822-H-PK
L-ALANINE (13C3, 99%)	Cambridge Isotope Laboratories	Cat# CLM-2184-H-PK
SODIUM D-3-HYDROXYBUTYRATE (13C4, 99%)	Cambridge Isotope Laboratories	Cat# CLM-3853-PK
SODIUM PALMITATE (U-13C16, 98%+)	Cambridge Isotope Laboratories	Cat# CLM-6059-PK
OLEIC ACID, SODIUM SALT (U-13C18, 98%)	Cambridge Isotope Laboratories	Cat# CLM-8763-PK
LINOLEIC ACID, POTASSIUM SALT (U-13C18, 98%)	Cambridge Isotope Laboratories	Cat# CLM-8835-PK
L-SERINE (13C3, 99%)	Cambridge Isotope Laboratories	Cat# CLM-1574-H-PK
L-GLYCINE (13C2, 97-99%)	Cambridge Isotope Laboratories	Cat# CLM-1017-PK
CITRIC ACID (13C6, 99%)	Cambridge Isotope Laboratories	Cat# CLM-9021-PK
SODIUM ACETATE (1,2-13C2, 99%)	Cambridge Isotope Laboratories	Cat# CLM-440-PK
L-LEUCINE (13C6, 99%)	Cambridge Isotope Laboratories	Cat# CLM-2262-H-PK
L-VALINE (13C5,99%)	Cambridge Isotope Laboratories	Cat# CLM-2249-H-PK
L-ISOLEUCINE (13C6, 99%)	Cambridge Isotope Laboratories	Cat# CLM-2248-H-PK
L-HISTIDINE:HCL:H2O (13C6, 97-99%; 15N3, 97-99%)	Cambridge Isotope Laboratories	Cat# CNLM-758-PK
L-LYSINE (13C6, 99%; 15N2, 99%)	Cambridge Isotope Laboratories	Cat# CNLM-291-H-PK
L-METHIONINE (13C5, 99%; 15N, 99%)	Cambridge Isotope Laboratories	Cat# CNLM-759-H-PK
L-PHENYLALANINE (13C9, 99%; 15N, 99%)	Cambridge Isotope Laboratories	Cat# CNLM-575-H-PK
L-THREONINE (13C4, 97-99%; 15N, 97-99%)	Cambridge Isotope Laboratories	Cat# CNLM-587-PK
L-TRYPTOPHAN (13C11, 99%; 15N2, 99%)	Cambridge Isotope Laboratories	Cat# CNLM-2475-PK
Fatty acid free BSA	Sigma	Cat# A6003
Glycerokinase	Sigma	Cat# 6278
EDC	Sigma	Cat# 03449
3-Nitrophenylhydrazine	Sigma	Cat# N21804
Pyridine	Sigma	Cat# 270970
beta-mercaptoethanol	Sigma	Cat# M6250
Experimental Models: Organisms/Strains		
Mouse: C57BL/6	Charles River Laboratories	Cat #027
Software and Algorithms		
El-MAVEN software	Elucidata	https://resources.elucidata.io/elmaven
AccuCor	GitHub	https://github.com/XiaoyangSu/AccuCor
Other		
XBridge BEH Amide XP column	Waters	Cat# 176002889
Acquity UPLC BEH C18 column	Waters	Cat# 186003719
PicoLab Rodent Diet 20	LabDiet	Cat# 5053
Ketogenic Diet	Bio-Serv	Cat# F3666
Insulin ELISA Kit	Crystal Chem	Cat# 90080

RESOURCE AVAILABILITY

Lead Contact

Further information and requests for resources and reagents should be directed to and will be fulfilled by the Lead Contact, Joshua D. Rabinowitz (joshr@princeton.edu).

Materials Availability

This study did not generate new unique reagents.

Data and Code Availability

The MATLAB codes for the calculation of direct contributions with the constraint of non-negative values and for the quantification of absolute flux between circulating nutrients are available on GitHub: https://github.com/tonyshenghui/Flux_CircMet.

EXPERIMENTAL MODEL AND SUBJECT DETAILS

Mouse studies followed protocols approved by the Animal Care and Use Committee for Princeton University and for the University of Pennsylvania. *In vivo* infusions were performed on 12-14 week old C57BL/6 mice pre-catheterized in the right jugular vein (Charles River Laboratories, Wilmington, MA). Animals received either a normal chow diet (PicoLab Rodent 20 5053; laboratory Diet, St. Louis, MO) or a ketogenic diet (Bio-Serv F3666; Flemington, NJ). Mice were allowed at least 5 days of acclimation to the facilities prior to experimentation and were randomly chosen for infusions of different tracers. No blinding was implemented. Those animals receiving the ketogenic diet were adapted to the diet for at least 21 days before experimentation. The mice were on normal light cycle (8 AM – 8 PM). On the day of infusion experiment, mice were transferred to new cages without food around 9 AM (beginning of their sleep cycle) and infused for 2.5 h starting at around 3 PM. To probe the fed state, the mice were maintained without food until around 8 PM, at which time chow was placed back in the cages and the 2.5 h infusion initiated. The infusion setup (Instech Laboratories, Plymouth Meeting, PA) included a swivel and tether to allow the mouse to move around the cage freely. Water-soluble isotope-labeled metabolites (Cambridge Isotope Laboratories, Tewksbury, MA) were prepared as solutions in sterile normal saline. To make ^{13}C-labeled fatty acid solutions, the fatty acids were complexed with bovine serum albumin in a molar ratio 4:1. Infusion rate was set to 0.1 μL min^{-1} g^{-1} for water-soluble metabolites and 0.4 μL min^{-1} g^{-1} for fatty acids. Blood was collected by tail snip ($\sim$10 μL) and transferred into blood collection tubes with clotting factor (Sarstedt 16.442.100). Blood samples were stored on ice and then centrifuged at 16,000 x g for 10 min at 4°C to get serum samples. Tissue harvest was performed at the end of the infusion after euthanasia by cervical dislocation. Tissues were quickly dissected, clamped with a pre-cooled Wollenberger clamp, and dropped in liquid nitrogen.

METHOD DETAILS

Metabolite Extraction of Serum

Serum (2 μL) was added to 68 μL of −80°C 100% methanol, vortexed, and put on dry ice for at least 5 min. This mixture was then centrifuged at 16,000 x g for 10 min at 4°C and supernatant was mixed 1:1 with 80% methanol. After centrifugation again at 16,000 x g for 10 min at 4°C, the supernatant was transferred to tubes for LC-MS analysis.

Metabolite Extraction of Tissue

Frozen tissue was ground by a Cyromill at cryogenic temperature (Retsch, Newtown, PA). Ground tissue was then weighed ($\sim$20 mg) and mixed with −20°C 40:40:20 methanol:acetonitrile:water with 0.5% formic acid (extraction solvent) at a concentration of 25mg/mL. Samples were briefly vortexed before neutralizing with 8 μL of 15% ammonium bicarbonate per 100 μL of extraction solvent. Extract was then vortexed and centrifuged twice at 16,000 x g for 20 min at 4°C before the final supernatant was transferred to LC-MS tubes for analysis.

Metabolite Measurement by LC-MS

A quadrupole-orbitrap mass spectrometer (Q Exactive, Thermo Fisher Scientific, San Jose, CA) operating in negative mode was coupled to hydrophilic interaction chromatography (HILIC) via electrospray ionization. Scans were performed from m/z 70 to 1000 at 1 Hz and 140,000 resolution. LC separation was on a XBridge BEH Amide column (2.1 mm x 150 mm x 2.5 mm particle size, 130 Å pore size; Waters, Milford, MA) using a gradient of solvent A (20 mM ammonium acetate, 20 mM ammounium hydroxide in 95:5 water:acetonitrile, pH 9.45) and solvent B (acetonitrile). Flow rate was 150 μL/min. The LC gradient was: 0 min, 85% B; 2 min, 85% B; 3 min, 80% B; 5 min, 80% B; 6 min, 75% B; 7 min, 75% B; 8 min, 70% B; 9 min, 70% B; 10 min, 50% B; 12 min, 50% B; 13 min, 25% B; 16 min, 25% B; 18 min, 0% B; 23 min, 0% B; 24 min, 85% B. Autosampler temperature was 5°C, and injection volume was 5-10 μL for serum samples and 15 μL for tissue samples.

Circulating glycerol labeling was determined by first converting serum glycerol to glycerol-3-phosphate using glycerol kinase and then measuring the labeling of glycerol-3-phosphate with LC-MS.

Acetate was derivatized and measured by LC-MS. The derivatizing reagent was 12 mM EDC, 15 mM 3-Nitrophenylhydrazine and pyridine (2% v/v) in methanol. Reaction was stopped with quenching reagent consisting of 0.5 mM beta-mercaptoethanol and 0.1% formic acid in water. Serum (5 μL) was mixed with derivatizing reagent (100 μL) and incubated for 1 h at 4°C. Then, the samples were centrifuged at 16,000 x g for 10 min at 4°C, and 20 μL of supernatant was mixed with 200 μL of the quenching reagent. After centrifugation at 16,000 x g for 10 min at 4°C, supernatants were collected for LC-MS analysis. A quadrupole-time of flight mass spectrometer (Q-TOF; Agilent, Santa Clara, CA) operating in negative ion mode was coupled to C18 chromatography via electrospray ionization and used to scan from m/z 100 to 300 at 1 Hz and 15,000 resolution. LC separation was on an Acquity UPLC BEH C18 column (2.1 mm x 100 mm, 1.7 5 μm particle size, 130 Å pore size; Waters, Milford, MA) using a gradient of solvent A (water) and

solvent B (methanol). Flow rate was 200 μL/min. The LC gradient was: 0 min, 10% B; 1 min, 10% B; 5 min, 30% B; 7 min, 100% B; 11 min, 100% B; 11.5 min, 10% B; 14 min, 10% B. Autosampler temperature was 5°C, column temperature was 60°C and injection volume was 10 μL. Ion masses for derivatized acetate was 194.0571.

El-Maven (Elucidata) was used for analysis of LC-MS data. Isotope labeling was corrected using AccuCor, available on GitHub: https://github.com/XiaoyangSu/AccuCor.

Indirect Calorimetry

Indirect calorimetry was performed in individually housed mice using a 20-channel open-circuit indirect calorimeter, in which 10 cages were mounted inside two thermally controlled cabinets, maintained at 22°C (Comprehensive Lab Animal Monitoring System; Columbus Instruments, Columbus, OH, USA). After overnight acclimation (20 h), oxygen consumption (VO2), the amount of carbon dioxide produced (VCO2), energy expenditure, food and water intake, ambulatory and locomotor activity (infrared beam breaks) were determined during an initial period of fasting (9am-5pm), as well as for the following 40 h wherein mice were fed *ad libitum*. Average respiratory exchange ratio (RER) was calculated as the ratio of VCO2:VO2 over 48 h. Energy expenditure was calculated as heat (kcal/h) = (3.815 +1.232 x RER) x VO2). The metabolic studies were performed at the Penn Diabetes Research Center Rodent Metabolic Phenotyping Core (University of Pennsylvania).

Insulin Measurement

Serum insulin levels were measured using a commercially available ELISA-based assay kit (Crystal Chem, Cat# 90080).

QUANTIFICATION AND STATISTICAL ANALYSIS

Calculation of Average Dietary Fluxes

The indirect calorimetry determined that the energy expenditure was 0.39 ± 0.02 Calories/day/g for mice on the carbohydrate diet (CD) and 0.53 ± 0.04 Calories/day/g for mice on the ketogenic diet (KD). Using the calorie density for the diets (3.41 Calories/g for CD and 7.24 Calories/g for KD), we have the total dietary fluxes as 0.115 g CD/g of mouse/day and 0.073 g KD/g of mouse/day.

The average dietary fluxes for individual ingredients for mice on a diet are then calculated by using the total dietary fluxes and the composition of the diets (CD: PicoLab Rodent Diet 20 5053; KD: Bio-serv F3666). The diet formulas report combined glutamine + glutamate, which provides an upper bound on glutamine. The diet formulas specify the content of total saturated fatty acids, but not specific saturated fatty acids. Palmitic acid (C16:0) and oleic acid dietary flux is based on our measurement that palmitic acid and stearic acid (C18:0) are the main saturated fatty acids, with a ratio of 2.4:1 for CD and 1.7:1 for KD. The palmitic acid dietary flux was calculated based on this number for each diet. Other amino acids (other AAs) include arginine, aspartate, asparagine, cystine, proline, and tyrosine. The dietary flux for other fatty acids (other FAs) was calculated as the total dietary flux of fatty acids minus the sum of the dietary fluxes of palmitic acid, oleic acid, and linoleic acid.

Definition of F_{circ} and F_{circ}^{atom}

To measure the circulatory turnover flux of a nutrient with a carbon number of C, the uniformly ^{13}C-labeled form of the nutrient is infused. At steady state, the fraction of the labeled form $[M+i]$ of the nutrient in serum is measured as $L_{[M+i]}$. (Note that there are a total number of $C+1$ labeled forms for the nutrient, such that i is from 0 to C.) The circulatory turnover flux F_{circ} is defined as

$$F_{circ} = R \cdot \frac{1 - L_{[M+C]}}{L_{[M+C]}}, \quad \text{(Equation 3)}$$

where R is the infusion rate of the labeled tracer.

The carbon-atom circulatory turnover flux F_{circ}^{atom} of the nutrient is defined as

$$F_{circ}^{atom} = C \cdot R \cdot \frac{1 - L}{L}, \quad \text{(Equation 4)}$$

where L is the fraction of labeled carbon atoms in the nutrient, or mathematically

$$L = \frac{\sum_{i=0}^{C} i \cdot L_{[M+i]}}{C}. \quad \text{(Equation 5)}$$

As the definitions show, F_{circ} measures the turnover of the whole carbon skeleton of the molecule while F_{circ}^{atom} measures the turnover of the carbon atoms in the molecule.

Definition of Normalized Labeling

In the infusion of a ^{13}C-labeled tracer X, the normalized labeling of a nutrient Y is defined as $L_{Y \leftarrow X} = \frac{L_Y}{L_X}$, where L_X and L_Y are the fraction of labeled carbon atoms for X and Y, respectively, defined in Equation 5.

Calculation of Direct Contributions with the Constraint of Non-negative Values

As explained in the main text, by constructing a set of linear equations, we can solve them for the direct contribution from each of the circulating nutrients to a specific circulating nutrient (Equation 1) or the direct contribution from each circulating nutrient to the tissue TCA cycle (Equation 2). Due to measurement errors, the direct contributions calculated in this manner are sometimes negative, albeit with small values, which are not feasible. To obtain the direct contributions that best reflect the biological fluxes, we use an optimization procedure to search for the set of direct contributions (represented as vector f) that minimize the Euclidean distance between the predicted labeling (represented as vector $M \cdot f$) and the measured labeling (represented as vector L), under the constraint of non-negative f. Or mathematically,

$$\min \|M \cdot f - L\| \textit{with respect to } f \textit{ such that } f > 0$$

The optimization was performed using MATLAB function fmincon.

To estimate the errors for the values in f, we ran the optimization many times (with n = 100). For each optimization, instead of using the mean for each entry of the matrix M and the vector L, we sampled a value from a normal distribution with the mean and the standard deviation equal to the mean and the error in that entry. Each optimization resulted in a value for each entry of the vector f. The standard deviation of the n number of values (from n optimizations) for an entry in f was taken as its error.

Quantification of Absolute Flux between Circulating Nutrients

See Methods S1 in the Supplemental Information.